International Journal of Computational Methods and Experimental Measurements
https://www.acadlore.com/journals/IJCMEM

Numerical Analysis of Geogrid-Encased Stone Column Performance Mechanism in Al-Fao Soft Clay

Marwah Fadhil Al-Ghaith*, Osamah S. Abdulkareem Al-Salih, Samoel Mahdi Saleh

Department of Civil Engineering, College of Engineering, University of Basrah, 61004 Basrah, Iraq

* Correspondence: Marwah Fadhil Al-Ghaith (marwa.fadil@uobasrah.edu.iq)

Received: 01-20-2026 **Revised:** 03-04-2026 **Accepted:** 03-19-2026

Citation: M. F. Al-Ghaith, O. S. A. Al-Salih, and S. M. Saleh, "Numerical analysis of geogrid-encased stone column performance mechanism in Al-Fao soft clay," *Int. J. Comput. Methods Exp. Meas.*, vol. 14, no. 1, pp. 141–155, 2026. https://doi.org/10.56578/ijcmem140109.

Abstract: The alluvial clay deposits at Al-Fao, Southern Iraq, with deep soft clay, offer a great foundation challenge due to low bearing capacity and high risk of settlements. To address these issues, this study evaluated the performance mechanism of floating geogrid-encased stone columns (GESCs) through three-dimensional finite element analysis using PLAXIS 3D with a hardening soil (HS) constitutive model. A parametric study was conducted based on column diameter (0.4–0.8 m), a slenderness ratio (L/D = 3–30), and encasement lengths of (1/3 L, 2/3 L, and Full L). The results demonstrated that increasing the column diameter is the most effective strategy, achieving a maximum bearing capacity ratio (BCR) of 1.75 compared to unimproved soil. Notably, the findings revealed that a 2/3 L partial encasement provides performance nearly identical to full-length encasement (with a difference of less than 0.5%) while significantly reducing material costs by 33%. The geogrid encasement provided an improvement factor (IF) of 1.09 over ordinary stone columns (OSCs). This efficiency is attributed to the encasement's ability to restrain bulging failure within the upper active zone. The study concluded that 2/3 L partial encasement offers superior technical and economic benefits for floating systems in deep soft clay deposits.

Keywords: Al-Fao soft clay; Bearing capacity; Finite element analysis; Soil model; Partial encasement; Ground improvement

1 Introduction

The need for robust infrastructure in rapidly developing urban and economic centers necessitates construction in soils with challenging geotechnical conditions. The presence of large amounts of soft clay deposits in Southern Iraq makes the area vulnerable to differential settlement due to its low shear strength and susceptibility to differential settlement issues [1, 2].

Ordinary Stone Columns (OSCs) are widely used to accelerate settlement through drainage and improve bearing capacity through soil replacement [3–6]. However, these extremely soft clays severely restrict their effectiveness. Excessive bulging failure, which usually occurs in the upper part of the column, is caused by insufficient lateral confinement from the surrounding soil [2–11].

To address this mechanical instability, the geogrid-encased stone column (GESC) system was developed to offer supplementary confining pressure to the existing structure [12]. The purpose of the encasement is to provide a circumferential tension element to produce hoop stresses that maintain the stability of the granular column and improve the load transfer mechanism [13–16].

Reliable prediction of the behavior of these compositing systems requires advanced numerical tools. Recent studies have highlighted the efficacy of finite element simulation, combined with advanced stress-strain constitutive models, in capturing the nonlinear response of complex engineering materials [17]. However, traditional analysis based on an elastoplastic model might not precisely predict these responses because it may not be capable enough for these soft clays. So, three-dimensional modeling using the hardening soil (HS) model is necessary [18–20]. Recent studies have further demonstrated that advanced numerical modeling is crucial for accurately capturing the complex geotechnical behavior and stiffness degradation of encased stone columns in soft clay soils [21].

Despite the extensive literature on encased columns, significant knowledge gaps remain regarding their application in the specific deep soft deposits of the Basrah region. At present, the literature lacks thorough numerical analyses

concerning the following aspects: (1) calibration of GESC behavior to the specific geotechnical characteristics of Al-Fao soft clay; (2) stability assessments of floating columns with L/D ratios of up to 30, typical of deep deposits. Although contemporary research has explored the behavior of floating stone columns reinforced with geogrid encasement [22], data on their performance at such ultra-slender ratios in high-plasticity alluvial clays remain limited; and (3) optimization of partial encasement to economically limit bulging. This focus on optimization directly aligns with the growing trend in recent geotechnical literature toward evaluating the failure modes and cost considerations of geogrid encasements for sustainable design [23].

The primary novelty of this research lies in establishing the generalized performance mechanism of ultra slender floating GESCs (L/D up to 30), where reaching a firm stratum is impractical. Unlike previous studies that focus on end-bearing columns, this study provides a calibrated threshold for partial encasement, balancing the technical requirements for preventing bulging failure with the economic constraints of deep-ground improvement. Furthermore, while the model is calibrated for the Al-Fao region, the resulting dimensionless framework (BCR and IF) allows these findings to be applied to similar deep alluvial clay profiles globally.

2 Methodology and Numerical Modeling

To explain the mechanism of GESC used in the soft clay soil of Al-Fao, a three-dimensional finite element analysis was carried out using the PLAXIS 3D software (Version 2024).

2.1 Model Geometry

To create the three-dimensional finite-element model of the single stone column and the clay, PLAXIS 3D software (Version 2024) was used, as shown in Figure 1. By using this modeling technique, a good compromise is realized between computing time and the accuracy of the failure mechanism of the column.

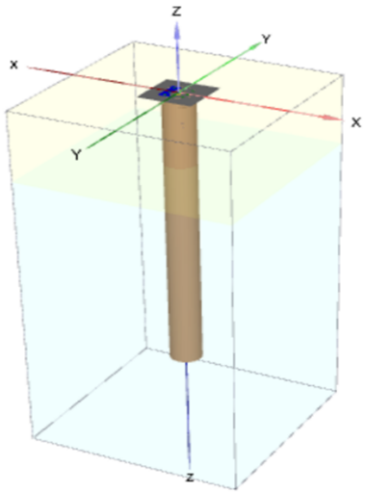

Figure 1. The stone column system

To reduce the effects of the boundary conditions and ensure that the confinement state around the column is consistent, the dimensions of the numerical domains were specified based on the column diameter (D) and length (L). For the cases analyzed, the boundaries were extended laterally to ensure that the width-to-column diameter ratio (W/D) ranged between 5 and 15. This was determined by the range of model widths used (4 m and 6 m) and the column diameters (0.4 m and 0.8 m), accounting for the effects of the area replacement ratio [9]. The adopted W/D range of 5 to 15 was explicitly chosen to prevent any artificial lateral confinement from the rigid boundaries. Preliminary boundary checks confirmed that within these specific lateral extents, the induced stress bulbs and plastic yielding zones are fully accommodated inside the numerical domain, thereby reflecting a realistic field response without boundary interference (see Figure 2). To model the deep deposits of the soft clay characteristic of the Al-Fao area, the model height (H) ranged between 12 m and 18 m. This selection allows for sufficient soil beneath the toe of the shortest column for dissipation of the stresses around it, along with realistic flotation for the other columns, even for the longest column length of 12 m.

Accordingly, the external boundaries were defined: 4 × 4 m to 6 × 6 m, and the vertical heights of 12 m and 18 m. This satisfies the requirements of numerical modeling for reducing the effects of boundaries around the model [18, 24].

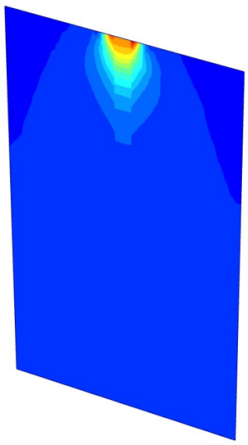

Figure 2. The stress bulbs in a stone column model

2.2 Material Properties and Constitutive Models

2.2.1 Al-Fao soft clay and interfaces

The highly compressible, moisture-sensitive Al-Fao soft clay was modeled using the advanced HS model [18, 25]. This model was selected over the simpler Mohr-Coulomb criterion due to its superior ability to simulate the non-linear, stress-dependent stiffness behavior typical of soft clays. The three most important stiffness parameters describing the properties of the model are E_{50}^{ref}, E_{oed}^{ref}, and E_{ur}^{ref}. The primary limitation of simpler elastoplastic models, such as Mohr-Coulomb, is the assumption of a constant Young's modulus (E), which fails to account for the increase in soil stiffness with depth in deep alluvial deposits. In the case of Al-Fao clay, where the soft layer extends to significant depths, the HS model's power-law stress dependency ensures a more realistic simulation. By incorporating separate modules for triaxial loading (E_{50}), oedometer compression (E_{oed}), and unloading-reloading (E_{ur}), the model accurately captures the non-linear settlement and the complex soil-column interaction during the bulging process, which a constant-stiffness model would likely overestimate. The properties of the borehole in this case study are as follows: a two-layer system, with the thickness of the first layer being 3 m , and the groundwater level being 1 m.

Interfaces with an interface stiffness ratio (R_{inter}) were introduced between the stone column and the surrounding clay to simulate the potential for slip and reduced shear transfer [18, 24]. All key geotechnical parameters for the HS model and interface properties are summarized in Table 1. These parameters were established based on comprehensive site investigation reports provided by the Consulting Engineering Bureau at the University of Basrah. The data were derived from specialized laboratory tests, including consolidated-undrained (CU) triaxial and oedometer tests, conducted on undisturbed samples from the Al-Fao region.

Table 1. The finite element parameters of Al-Fao soil

Properties	Symbol, Units	Layer 1	Layer 2
Material model	Type	Hardening soil	Hardening soil
Drainage type	Condition	Undrained (B)	Undrained (B)
Saturated unit weight	γ_{sat} (kN/m^3)	19.52	19.77
Unsaturated unit weight	γ_{unsat} (kN/m^3)	18.25	14.45
Secant stiffness	E_{50}^{ref} (kN/m^2)	1969	1648
Tangent stiffness	$E_{\text{oed}}^{\text{ref}}$ (kN/m^2)	1575	1319
Unloading/Reloading stiffness	$E_{\text{ur}}^{\text{ref}}$ (kN/m^2)	7458	5088
Poisson's ratio	ν_{ur}	0.15	0.15
Void ratio	e_{init}	0.71	0.89
Power for stress level	m	1	1
Undrained shear strength	$S_{u,\text{ref}}$ (kN/m^2)	42.5	34.5
Friction angle	φ' (degree)	-	-
Dilatancy angle	ψ° (degree)	-	-
Interface stiffness ratio	R_{inter}	0.9	0.9

2.2.2 Stone column material

The crushed stone aggregate was modeled as a linear elastic-perfectly plastic material with a Mohr-Coulomb failure criterion [14, 18, 24]. This model is deemed appropriate for representing the high-stiffness, frictional behavior of granular materials under the expected stress levels. Key parameters include the effective friction angle (φ'), cohesion (c'), and the dilation angle (ψ), which is critical for capturing the volumetric expansion during shear that mobilizes lateral confinement. The properties of the crushed stone were taken from the study [26], as shown in Table 2.

Table 2. Parameters of the crushed stone [26]

Properties	Symbol, Units	Value
Material model	Type	Mohr-Coulomb
Drainage type	Condition	Drained
saturated unit weight	γ_{sat} (kN/m^3)	16.5
Unsaturated unit weight	γ_{unsat} (kN/m^3)	15.7
Young's modulus	E (kN/m^2)	20000
Poisson's ratio	v_{ur}	0.3
Cohesion	c' (kN/m^2)	0.01
Friction angle	φ' (degree)	42
Dilatancy angle	ψ° (degree)	20
Interface stiffness ratio	R_{inter}	0.9

2.2.3 Geogrid encasement

The geogrid was modeled as a two-dimensional linear elastic structural element (geogrid element in PLAXIS 3D) capable of resisting axial tensile forces but offering no flexural stiffness [14, 18]. Its primary mechanical property is the axial stiffness (EA), which governs the magnitude of confining pressure generated to restrain column bulging. Based on a previous study [27], a geogrid type G3 with EA = 240 kN/m was used for all encasement simulations.

2.2.4 Footing

The surface footing 1 × 1 m was modeled as a linear elastic plate element. Its properties are provided in Table 3.

Table 3. Parameters of the crushed stone [26]

Properties	Symbol, Units	Value
Material	Type	Elastic
Thickness	d (m)	0.6
Unit weight	γ (kN/m^3)	24
Young's modulus	E^* (KN/m^2)	23.5 × 10^6
Poisson's ratio	v	0.2

Note: $*$ Depending on ACI Code (318M-11) ($E = 4700\sqrt{f'_c}$).

2.3 Finite Element Model Setup

2.3.1 Mesh design and boundary conditions

The domain was discretized using 10-noded tetrahedral elements (see Figure 3). A medium mesh density was applied globally, with local refinement around the stone column, encasement zone, and the upper section where bulging is anticipated. This ensured accuracy in regions of high stress and strain gradients. To verify that the numerical solutions are independent of the element size, a mesh sensitivity analysis was conducted before the final parametric study. Comparing coarse, medium, and fine configurations revealed that the variation in the ultimate bearing capacity between the locally refined medium mesh and the fine mesh was less than 2.5%. Therefore, the current mesh configuration was adopted to optimize computational time without compromising the precise capture of the failure mechanism. The final mesh consisted of approximately 13,261 soil elements and 21,186 nodes. Vertical boundaries were restrained in the horizontal direction, while the base was fixed in all directions. The top surface was kept free [14, 18].

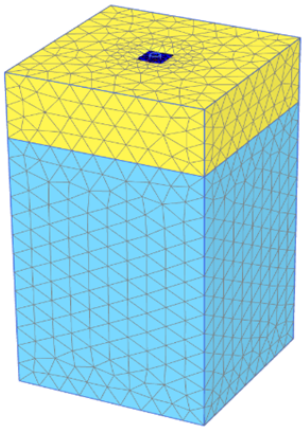

Figure 3. The 3D mesh of the model

2.3.2 Analysis stages and loading procedure

The numerical analysis was carried out through staged procedures in the PLAXIS 3D software to simulate the real-case scenario of the column's installation and subsequent loads as follows:

(1) Initial geostatic equilibrium: The original state of in-situ stress, with vertical and horizontal stresses dependent on the value of the coefficient of lateral earth pressure at rest K_0, was determined using the gravity loading method before any construction process [9, 18].

(2) Insertion of stone columns: The soil components were replaced by the stone column material through the volume replacement technique [18, 24].

(3) Geogrid application: The geogrid encasement was applied by activating the geogrid elements [14, 18] along the length of the column as designated for partial and full encasements (see Figure 4). The geogrid component, along with the interface stiffness ratio (Rinter), was also turned on to account for geogrid and stone column interaction.

(4) Loading stage: The footing received a uniform vertical pressure. The loading was performed using displacement control of 120 mm rather than load control. This approach allows for the precise capture of the failure mechanism and, hence, the ultimate bearing capacity [18, 19].

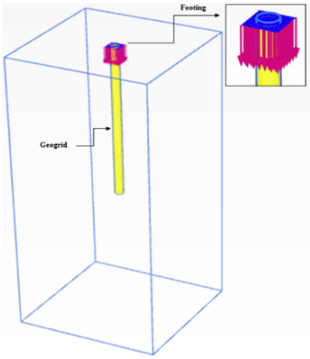

Figure 4. Illustration of the geogrid in the model

2.4 Model Validation

Before starting the parametric analysis on Al-Fao clay, a thorough validation process was carried out by comparing the numerical results with published experimental data to ensure the precision and dependability of the numerical model in PLAXIS 3D. The procedure involved replicating a reference model related to the performance of unreinforced soil and OSC by Al-Qayssi [7] and GESC by Yoo and Lee [28], in soft soil. The actual geometric properties and material characteristics, as well as the boundary conditions, as presented in the reference model, were directly incorporated to create a numerical load-versus-settlement curve.

Figure 5 and Figure 6 present the comparison between the numerically predicted load-settlement behavior and the experimental measurements. The results demonstrate a good agreement across all cases, accurately capturing both the initial stiffness and the ultimate capacity trends. Quantitatively, the discrepancy between the numerical and experimental results at maximum settlement was minimal. The deviation was found to be 4.8% for the unreinforced

soil and 2.64% for the OSC based on Al-Qayssi's data [7], and 4.76% for the GESC compared with Yoo and Lee's data [28].

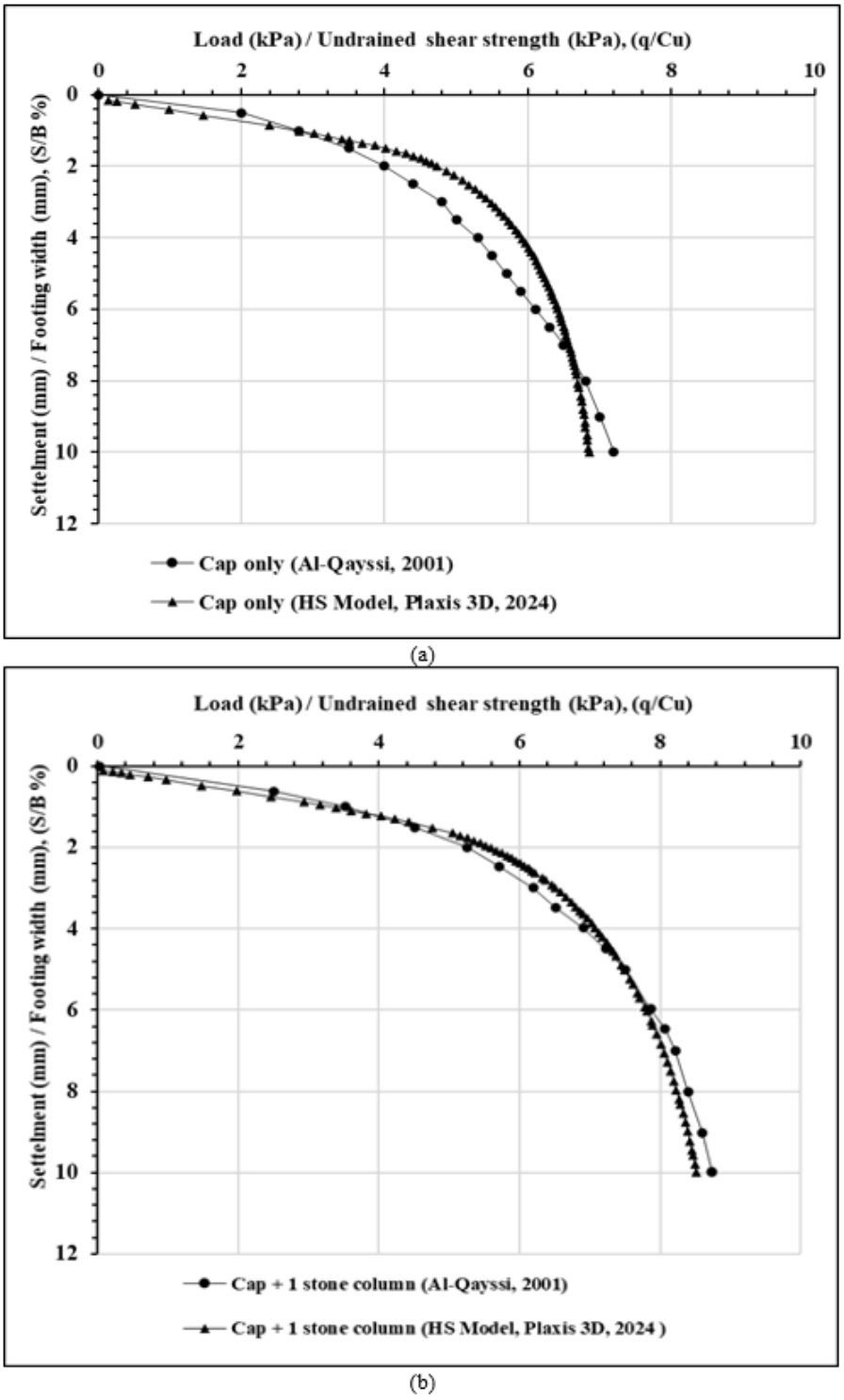

Figure 5. The verification model result of the case study [7]: (a) with cap only; (b) with cap + stone column

This difference of less than 5% highlights the excellent precision of the results. Even more important, the results correctly capture the main features of the problem: large settlement reduction for the OSC compared with the unreinforced soil, and a large additional improvement provided by the geogrid encasement for the GESC. This excellent comparison, both qualitative and quantitative, vindicates the choice of the numerical model components: the HS model for the clay, the Mohr-Coulomb model for the crushed stone, the interface parameters, and the overall modeling approach.

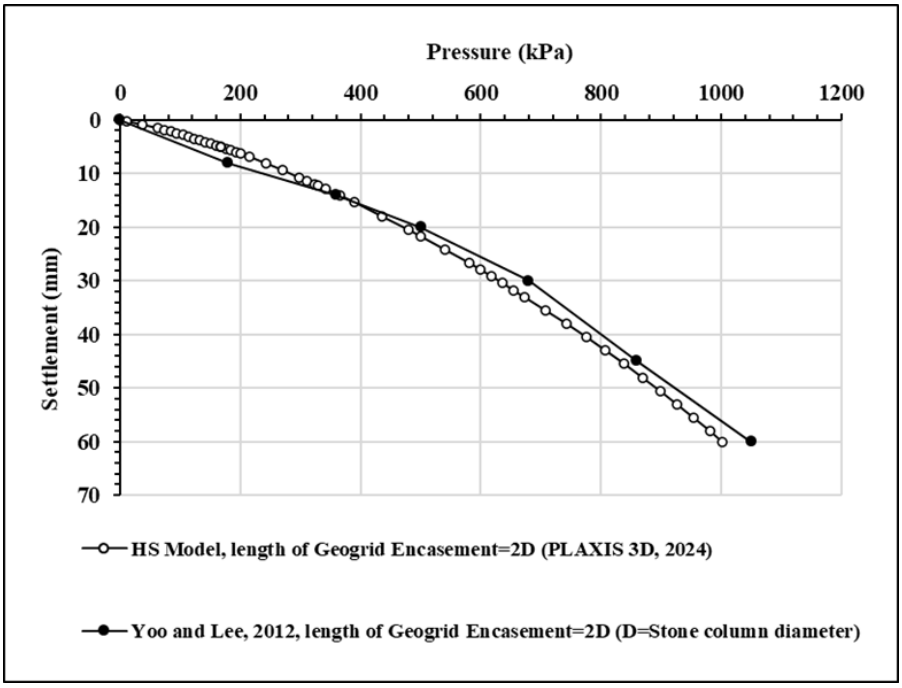

Figure 6. The verification model result of the case study [28]

It gives excellent confidence that the model behaves well for complex soil-column interaction problems, and that it is accordingly safe to use it for the parametric analysis of partially encased columns on the Al-Fao soft clay. While certain reference studies, such as a case study by Yoo and Lee [28], provide data on lateral column deformation (bulging), the current validation focuses specifically on the load-settlement response. This is justified as the bearing capacity and settlement control are the primary performance indicators and design criteria for ground improvement in the deep, soft deposits of the Al-Fao region. Furthermore, the strong correlation achieved in the load-settlement curves confirms that the fundamental soil-structure interaction and the geogrid-stone confinement mechanism are correctly captured by the model, providing a reliable basis for the subsequent parametric investigations.

3 Results and Discussion

This section presents the numerical results derived from the validated 3D Finite Element Model (PLAXIS 3D), discussing the performance of OSC and GESCs designed for the improvement of the Al-Fao soft clay soil. The initial bearing capacity of the unimproved soil was established as 255 kPa using the 0.1 B method [29], where B is the width of the footing; in this work, B is 1 m. This value serves as the baseline for calculating all improvement ratios.

3.1 Parametric study Overview

The parametric study in Al-Fao was designed to assess the influence of column geometry and encasement parameters on the bearing capacity of the single floating stone column. Columns with diameters (D) of 0.4, 0.6, and 0.8 m were analyzed across a wide range of lengths (L = 2.4, 3.2, 3.6, 4, 4.8, 6, 9, and 12 m), producing slenderness ratios (L/D) from 3 to 30. Furthermore, a specific geogrid type (G3) with an axial stiffness of EA = 240 kN/m [27] was examined under different casing lengths: partial (1/3 L, 2/3 L) and full-length (L) encasement.

The result of load-settlement curves for all configurations is shown in Figure 7, Figure 8, and Figure 9 for D = 0.4, 0.6, and 0.8 m, respectively. Table 4, Table 5, and Table 6 summarize the ultimate bearing capacities (q_{ult}). To facilitate a generalized, dimensionless interpretation of the results, making the findings applicable beyond the specific soil profile of Al-Fao, the performance is synthesized using two fundamental dimensionless metrics:

(1) Bearing capacity ratio (BCR): This parameter evaluates the overall ground improvement efficiency. It is defined as the ratio of the ultimate bearing capacity of the improved soil (qtreated) to that of the natural, unimproved Al-Fao clay (q_{treated}), which was determined to be 255 kPa.

$$BCR = \frac{q_{\text{treated}}}{q_{\text{untreated}}} \tag{1}$$

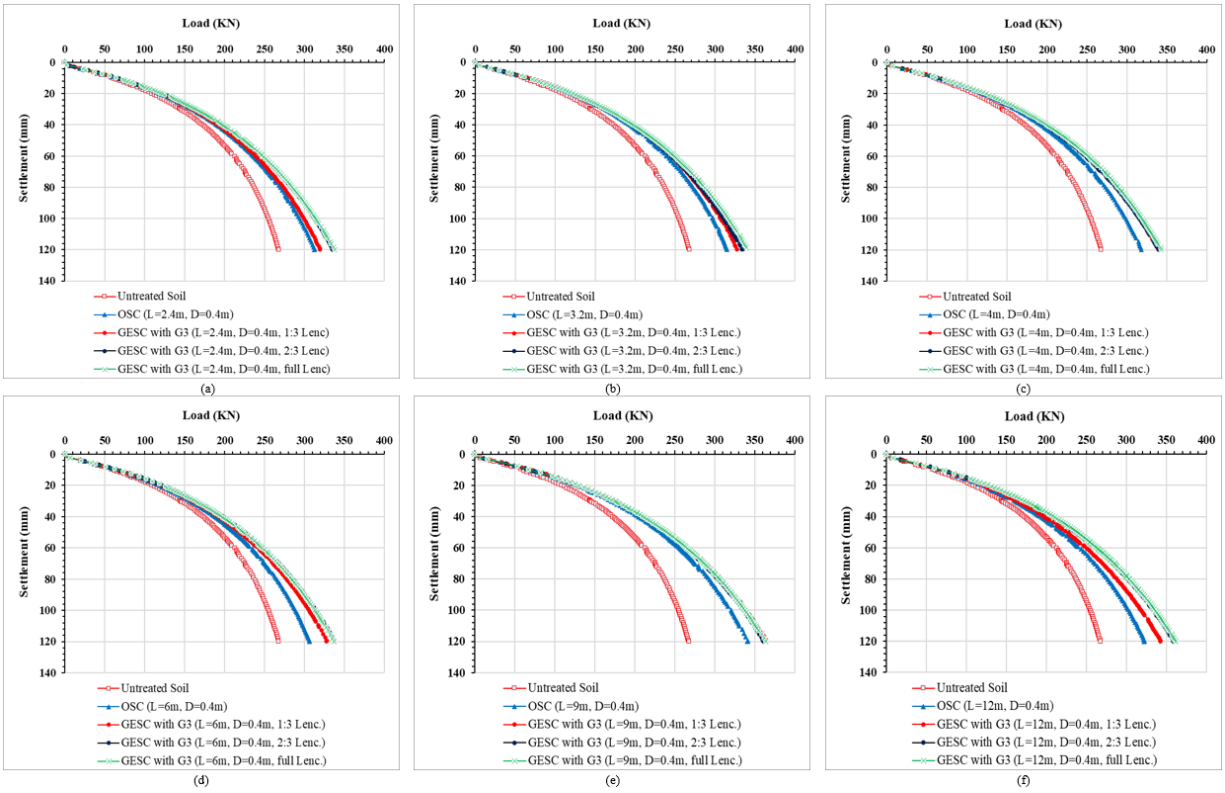

Figure 7. Load-settlement relationships for (D = 0.4 m): (a) L/D = 6; (b) L/D = 8; (c) L/D = 10; (d) L/D = 15; (e) L/D = 22.5; (f) L/D = 30

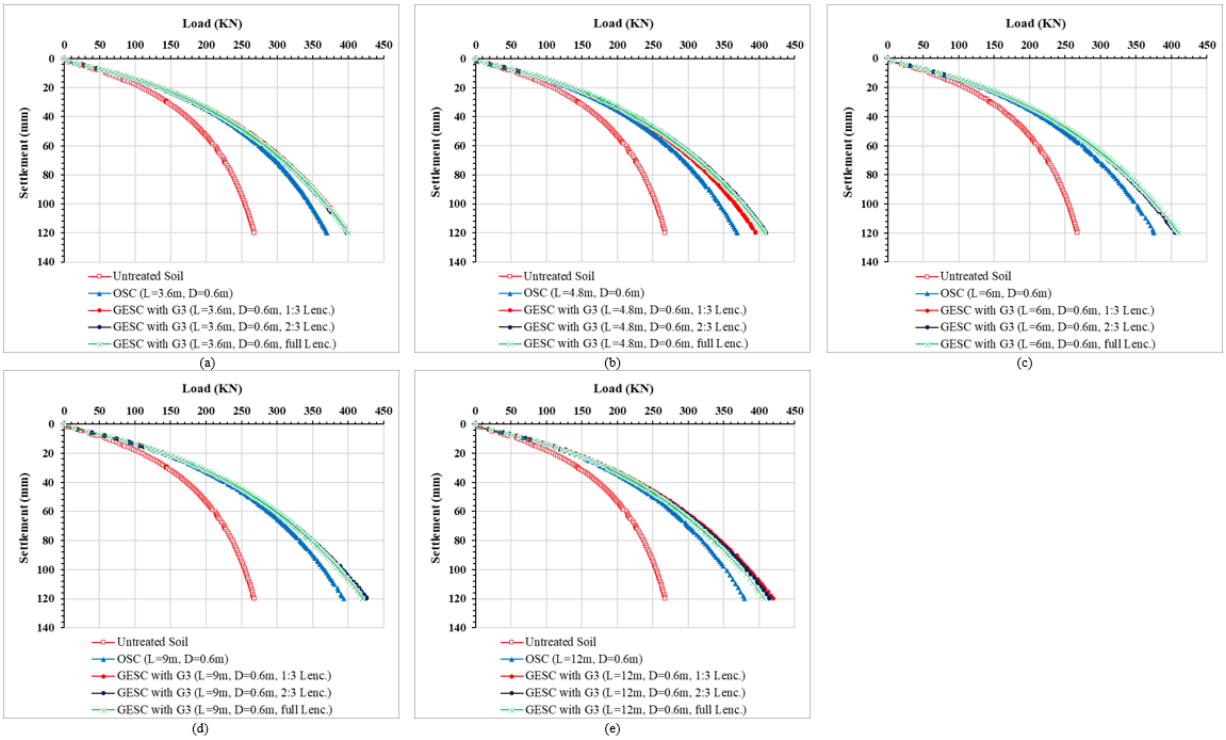

Figure 8. Load-settlement relationships for (D = 0.6 m): (a) L/D = 6; (b) L/D = 8; (c) L/D = 10; (d) L/D = 15; (e) L/D = 20

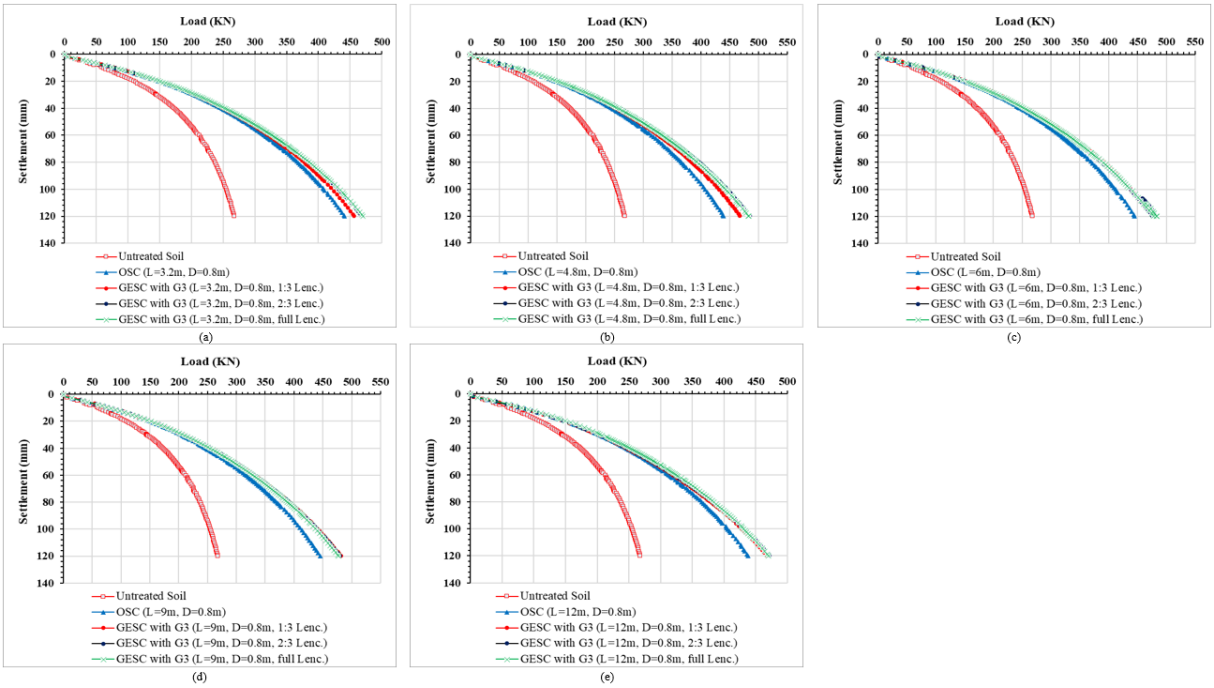

Figure 9. Load-settlement relationships for (D = 0.8 m): (a) L/D = 4; (b) L/D = 6; (c) L/D = 7.5; (d) L/D = 11.25; (e) L/D = 15

Table 4. Results for column diameter (D = 0.4 m)

Column Length (m)	Slenderness Ratio (L/D)	Encasement Configuration	Ultimate Bearing Capacity q_{ult} (kPa)	Bearing Capacity Ratio (BCR)	Improvement Factor (IF)
2.4	6	OSC (Uncased)	294	1.15	1.00
		GESC (1/3 L)	300	1.18	1.02
		GESC (2/3 L)	312	1.22	1.06
		GESC (Full L)	313	1.23	1.06
3.2	8	OSC (Uncased)	297	1.16	1.00
		GESC (1/3 L)	307	1.20	1.03
		GESC (2/3 L)	311	1.22	1.05
		GESC (Full L)	316	1.24	1.06
4	10	OSC (Uncased)	299	1.17	1.00
		GESC (1/3 L)	316	1.24	1.06
		GESC (2/3 L)	316	1.24	1.06
		GESC (Full L)	319	1.25	1.07
6	15	OSC (Uncased)	289	1.13	1.00
		GESC (1/3 L)	305	1.20	1.06
		GESC (2/3 L)	315	1.24	1.09
		GESC (Full L)	314	1.23	1.09
9	22.5	OSC (Uncased)	321	1.26	1.00
		GESC (1/3 L)	340	1.33	1.06
		GESC (2/3 L)	337	1.32	1.05
		GESC (Full L)	338	1.33	1.05
12	30	OSC (Uncased)	304	1.19	1.00
		GESC (1/3 L)	319	1.25	1.05
		GESC (2/3 L)	334	1.31	1.10
		GESC (Full L)	337	1.32	1.11

Notes: OSC = ordinary stone column; GESC = geogrid-encased stone column.

Table 5. Results for column diameter (D = 0.6 m)

Column Length (m)	Slenderness Ratio (L/D)	Encasement Configuration	Ultimate Bearing Capacity q_{ult} (kPa)	Bearing Capacity Ratio (BCR)	Improvement Factor (IF)
3.6	6	OSC (Uncased)	346	1.36	1.00
		GESC (1/3 L)	371	1.45	1.07
		GESC (2/3 L)	367	1.44	1.06
		GESC (Full L)	368	1.44	1.06
4.8	8	OSC (Uncased)	344	1.35	1.00
		GESC (1/3 L)	365	1.43	1.06
		GESC (2/3 L)	378	1.48	1.10
		GESC (Full L)	376	1.47	1.09
6	10	OSC (Uncased)	352	1.38	1.00
		GESC (1/3 L)	377	1.48	1.07
		GESC (2/3 L)	375	1.47	1.07
		GESC (Full L)	377	1.48	1.07
9	15	OSC (Uncased)	367	1.44	1.00
		GESC (1/3 L)	387	1.52	1.05
		GESC (2/3 L)	393	1.54	1.07
		GESC (Full L)	388	1.52	1.06
12	20	OSC (Uncased)	355	1.39	1.00
		GESC (1/3 L)	386	1.51	1.09
		GESC (2/3 L)	383	1.50	1.08
		GESC (Full L)	375	1.47	1.06

Notes: OSC = ordinary stone column; GESC = geogrid-encased stone column.

Table 6. Results for column diameter (D = 0.8 m)

Column Length (m)	Slenderness Ratio (L/D)	Encasement Configuration	Ultimate Bearing Capacity q_{ult} (kPa)	Bearing Capacity Ratio (BCR)	Improvement Factor (IF)
3.2	4	OSC (Uncased)	407	1.60	1.00
		GESC (1/3 L)	425	1.67	1.04
		GESC (2/3 L)	433	1.70	1.06
		GESC (Full L)	435	1.71	1.07
4.8	6	OSC (Uncased)	408	1.60	1.00
		GESC (1/3 L)	433	1.70	1.06
		GESC (2/3 L)	446	1.75	1.09
		GESC (Full L)	443	1.74	1.09
6	7.5	OSC (Uncased)	412	1.62	1.00
		GESC (1/3 L)	440	1.73	1.07
		GESC (2/3 L)	436	1.71	1.06
		GESC (Full L)	441	1.73	1.07
9	11.25	OSC (Uncased)	414	1.62	1.00
		GESC (1/3 L)	441	1.73	1.07
		GESC (2/3 L)	439	1.72	1.06
		GESC (Full L)	437	1.71	1.06
12	15	OSC (Uncased)	406	1.59	1.00
		GESC (1/3 L)	428	1.68	1.05
		GESC (2/3 L)	433	1.70	1.07
		GESC (Full L)	431	1.69	1.06

Notes: OSC = ordinary stone column; GESC = geogrid-encased stone column.

(2) Improvement factor (IF): To isolate the specific contribution of the geogrid encasement, the IF is utilized. It is defined as the ratio of the bearing capacity of the GESC (q_{GESC}) to that of an OSC (q_{OSC}) under identical geometric conditions. This dimensionless ratio specifically quantifies the efficiency of the reinforcement mechanism

and the mobilized confining pressure, independent of the area replacement effect.

$$IF = \frac{q_{GESC}}{q_{OSC}} \tag{2}$$

3.2 Analysis of Key Performance Mechanisms

3.2.1 Influence of column diameter (D) and area replacement

The numerical results, as synthesized in the summary plots (Figure 10 and Figure 11), reveal a nonlinear enhancement in the BCR as the column diameter increases. This trend is consistent across different encasement lengths, though the magnitude of improvement varies significantly:

• Small Diameter (D = 0.4 m): The improvement was relatively modest, with a peak BCR of 1.33 (observed at L = 9 m with 1/3 L encasement).

• Medium Diameter (D = 0.6 m): The efficiency increased notably, reaching a maximum BCR of 1.54 (at L = 9 m and 2/3 L encasement).

• Large Diameter (D = 0.8 m): The performance gains were most substantial, achieving a high BCR of 1.75 (at L = 4.8 m and 2/3 L encasement).

• Analysis of Performance Mechanism:

This significant improvement is primarily driven by the increase in the area replacement ratio, which alters the overall stiffness of the soil-column system. As the area replacement ratio increases, the Stress Concentration Ratio (SCR) rises, meaning the stiffer stone column attracts a higher proportion of the applied load, effectively 'shielding' the surrounding soft Al-Fao clay from excessive stresses. Furthermore, the larger diameter provides a greater circumferential surface area, which enhances the load transfer mechanism through interface skin friction. This allows for a more efficient distribution of stresses into deeper, more competent clay strata. From a confinement perspective, the larger diameter in GESCs enables the geogrid to mobilize higher hoop tension at smaller lateral strains. This increased lateral confinement restricts the bulging of the stone aggregates more effectively than in smaller diameters, thereby maintaining the structural integrity of the column under higher vertical loads [5, 9].

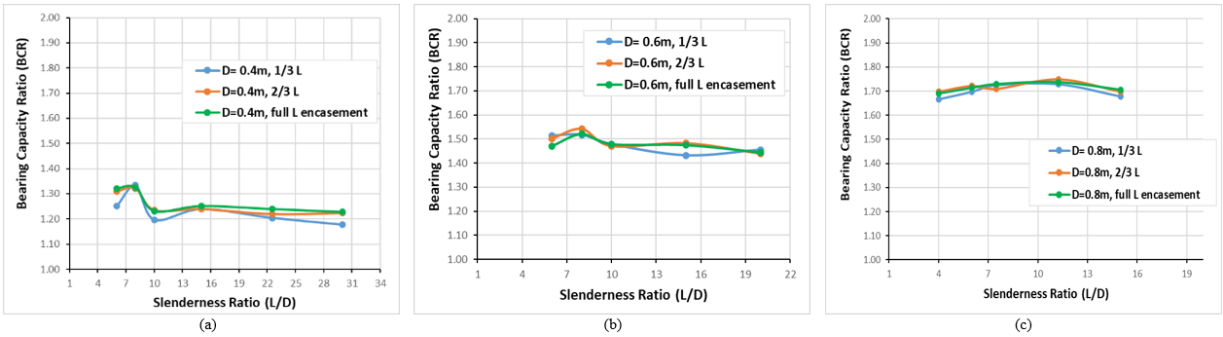

Figure 10. Variation of bearing capacity ratio (BCR) with slenderness ratio (L/D) for various encasement lengths: (a) D = 0.4 m; (b) D = 0.6 m; (c) D = 0.8 m

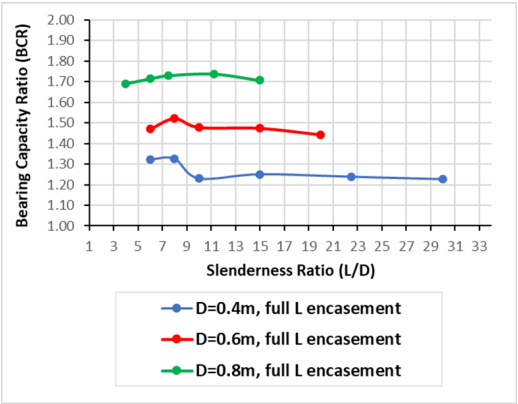

Figure 11. Influence of column diameter (D) on the bearing capacity ratio (BCR) trends for geogrid-encased stone columns (GESCs)

3.2.2 Efficiency of partial encasement (2/3 L vs. Full L)

One of the most important and economically significant findings of this research is that there is no performance difference between partial and full encasement for floating columns.

• Statistical Evidence: In a 2/3 L encasement with a diameter of 0.4 m, where L = 2.4 m, a value of 312 kPa in ultimate capacity was obtained compared to 313 kPa for full encasement. This represents a marginal difference of only 0.32%. Further, in a similar 2/3 L with a diameter of 0.8 m, with L being 3.2 m, a variation of less than 0.5% was established between 2/3 L and full-L encasement, which were 433 kPa and 435 kPa, respectively.

• Mechanical Interpretation: This confirms that the bulging failure is concentrated within the upper active zone (2D to 4D depth). Providing reinforcement beyond this critical depth (specifically beyond 2/3 L) does not contribute significantly to the ultimate capacity, as the lower portion of the column primarily transfers load through skin friction rather than resisting radial expansion [15].

3.2.3 Influence of a slenderness ratio (L/D)

As illustrated in the summary dimensionless plot (Figure 10 and Figure 11), beyond a critical slenderness ratio (L/D) of approximately 15, no additional advantage in BCR is observed. It implies the changeover in the loading response, and the column would be largely working as a floating column. The phenomenon matches the notion of a floating column as introduced by Dheerendra Babu et al. [5] and Barksdale and Bachus [10].

3.3 Quantitative Performance Comparison

3.3.1 Superiority of geogrid-encased stone column over ordinary stone column

Geogrid encasement significantly improves performance compared to OSCs. With a total bearing capacity of 446 kPa, the optimal configuration (D = 0.8 m, L = 4.8 m, 2/3 L encasement) outperformed unimproved soil (255 kPa) by a BCR of 1.75 and soil improved with OSCs (408 kPa) by an IF of 1.09. This IF of 1.09 is consistent with the results of the study by Yoo and Lee [28], clearly demonstrating the contribution of geogrid encasement in preventing premature bulging.

3.4 Synthesis of Improvement Mechanisms and Design Recommendations

The superior performance of the 2/3 L encased three mechanisms that drive the GESC system:

1. Hoop Stress Mobilization: The geogrid provides a stiff boundary condition, which imposes a radial restraint that suppresses the tendency of the stone aggregate to dome into the soft Al-Fao clay [15].

2. Stiffness Homogenization: The presence of confinement has been shown to improve the stiffness of stone columns, allowing them to resist a higher amount of vertical load with minimal shortening [3].

3. Stress Redistribution: The stiff inclusion affects vertical stress with n values greater than 1, thus relieving stress on the soft clay [8].

Figure 11 synthesizes the performance of the full encasement configuration across all column diameters, directly addressing the need for dimensionless parametric analysis. A clear engineering rule emerges: for any given slenderness ratio (L/D), a larger column diameter consistently yields a significantly higher BCR. This is due to the area replacement effect, which enhances stress concentration on the stiffer column and more efficiently mobilizes the confinement pressure within the soft Al-Fao clay deposit.

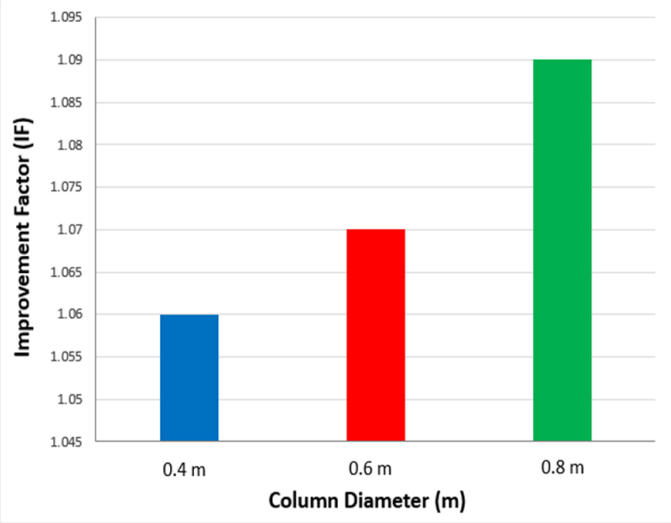

Figure 12. Evaluation of the net improvement factor (IF) across different column diameters

As illustrated in Figure 12, the effectiveness of the geogrid encasement (represented by IF) exhibits a positive correlation with the column diameter. The net gain from encasement increases as the diameter grows from 0.4 m to 0.8 m. This confirms that for larger-diameter columns, which are more prone to lateral bulging in the soft Fao clay, the confinement provided by the geogrid is more efficiently mobilized, yielding a higher relative improvement compared to OSC.

3.4.1 Practical design recommendations

To translate these findings into practice for the Al-Fao region, the following guidelines are proposed:

1. Optimal Encasement: Reinforcing only the top two-thirds (2/3 L) is recommended. This achieves 99% of the full-encasement benefit while providing a 33% saving in geogrid material costs.

2. Geometric Efficiency: Floating columns should be designed with an L/D ratio of 15. Lengths beyond this limit are not cost-effective.

3. Critical Zone: Construction quality control should focus on the upper 4D depth, where the geogrid's confinement effect is most vital for preventing settlement.

4 Conclusion

This study involves a numerical investigation of floating GESCs on the soft soil in Al-Fao. From the obtained parametric results, the most important conclusions are as follows:

(1) Geometric Optimization: Diameter is established to be the dominant variable for bearing-capacity increase based on the area replacement effect. The results show that by increasing the diameter to 0.8m, the BCR would reach the maximum at BCR = 1.75, showing that the resistance to lateral expansion is more efficient than the column length increase.

(2) Economical Design Limitation: It can be shown that encasing only two-thirds (2/3 L) of column length fully captures the critical bulging depth, which ranges from 2D to 4D. This allows achieving an almost identical improvement of 33% in comparison with fully encased GESC (difference $< 0.32\%$), reducing the consumption of geogrid.

(3) Limitations of Effectiveness (critical L/D): Performance decreases rapidly after reaching a certain critical value of slenderness ratio L/D ≈ 15, where further length increase has a negligible impact due to the transition from load-bearing to friction-type structure.

(4) Advantage of Mechanical Properties: As compared to conventional piles, geogrid improves pile performance by a factor of IF = 1.09. The mechanism behind it involves mobilizing hoop tensile stresses that allow maintaining the structural integrity of the stone aggregate.

(5) Application and Future Research: While the model presented shows good results for predicting the trends, in practice, implementation in Al-Fao should account for the smear effect. In the future, attention needs to be paid to experimental full-scale tests for the estimation of reduction factors and long-term behaviour.

Author Contributions

Conceptualization, M.F.A.-G. and O.S.A.A.-S.; methodology, M.F.A.-G. and O.S.A.A.-S.; validation, S.M.S. and O.S.A.A.-S.; formal analysis, M.F.A.-G.; investigation, M.F.A.-G.; resources, M.F.A.-G.; data curation, S.M.S. and M.F.A.-G.; writing—original draft preparation, M.F.A.-G.; writing—review and editing, O.S.A.A.-S. and S.M.S.; visualization, M.F.A.-G.; supervision, O.S.A.A.-S.; project administration, O.S.A.A.-S. All authors were actively involved in discussing the findings and refining the final manuscript.

Data Availability

The data used to support the findings of this study are available from the corresponding author upon request.

Conflicts of Interest

The authors declare no conflicts of interest.

References

[1] J. M. O. Hughes and N. J. Withers, "Reinforcing of soft cohesive soils with stone columns," *Ground Eng.*, vol. 7, no. 3, pp. 42–49, 1974.

[2] W. F. V. Impe, "Improvement of settlement behaviour of soft layers by means of stone columns," in *Proceedings of 8th European Conference on Soil Mechanics and Foundation Engineering: Improvement of Ground, Helsinki*, Helsinki, Finland, 1983, pp. 309–312.

[3] A. M. Abdelaziz, A. Elshesheny, N. Abdelmotaal, and N. M. Nagy, "Numerical behaviour of stone column in soft clayey soil," *IOP Conf. Ser.: Earth Environ. Sci.*, vol. 1396, p. 012005, 2024. https://doi.org/10.1088/1755-1315/1396/1/012005

[4] M. J. Al-Waily, N. K. Al-Saoudi, and M. S. Al-Qaisi, "Assessment the behavior of stone columns under confined compression," *IOP Conf. Ser.: Earth Environ. Sci.*, vol. 856, no. 1, p. 012033, 2021. https://doi.org/10.1088/1755-1315/856/1/012033

[5] M. R. Dheerendra Babu, S. Nayak, and R. Shivashankar, "A critical review of construction, analysis and behaviour of stone columns," *Geotech. Geol. Eng.*, vol. 31, no. 1, pp. 1–22, 2013. https://doi.org/10.1007/s10706-012-9555-9

[6] B. G. Sexton, B. A. McCabe, M. Karstunen, and N. Sivasithamparam, "Stone column settlement performance in structured anisotropic clays: The influence of creep," *J. Rock Mech. Geotech. Eng.*, vol. 8, no. 5, pp. 672–688, 2016. https://doi.org/10.1016/j.jrmge.2016.05.004

[7] M. R. M. Al-Qayssi, "Unreinforced and reinforced behaviour of single and groups of granular piles," phdthesis, University of Baghdad, Baghdad, Iraq, 2001.

[8] M. J. Al-Waily, "Stress concentration ratio of model stone columns improved by additives," phdthesis, University of Technology, Baghdad, Iraq, 2007. https://search.emarefa.net/detail/BIM-305458

[9] A. P. Ambily and S. R. Gandhi, "Behavior of stone columns based on experimental and FEM analysis," *J. Geotech. Geoenviron. Eng.*, vol. 133, no. 4, pp. 405–415, 2007. https://doi.org/10.1061/(ASCE)1090-0241(2007)133:4(405)

[10] R. D. Barksdale and R. C. Bachus, "Design and construction of stone columns," U.S. Department of Transportation, 1983. https://rosap.ntl.bts.gov/view/dot/25319/dot_25319_DS1.pdf

[11] B. A. McCabe, G. J. Nimmons, and D. Egan, "A review of field performance of stone columns in soft soils," *Proc. Inst. Civ. Eng. Geotech. Eng.*, vol. 162, no. 6, pp. 323–334, 2009. https://doi.org/10.1680/geng.2009.162.6.323

[12] M. Raithel and H. G. Kempfert, "Calculation models for dam foundations with geotextile coated sand columns," in *Proceedings of ISRM International Symposium*, Melbourne, Australia, 2000, pp. 19–24.

[13] P. Bhatia and M. Hasan, "Three-dimensional numerical investigation of stone columns encased with geosynthetic in very soft soil," in *Proceedings of Indian Geotechnical Conference*, Aurangabad, India, 2024, pp. 503–515. https://doi.org/10.1007/978-981-96-2444-7_39

[14] S. N. Malarvizhi, "Comparative study on the behavior of encased stone column and conventional stone column," *Soils Found.*, vol. 47, no. 5, pp. 873–885, 2007. https://doi.org/10.3208/sandf.47.873

[15] S. Murugesan and K. Rajagopal, "Geosynthetic-encased stone columns: Numerical evaluation," *Geotext. Geomembr.*, vol. 24, no. 6, pp. 349–358, 2006. https://doi.org/10.1016/j.geotexmem.2006.05.001

[16] S. Murugesan and K. Rajagopal, "Studies on the behavior of single and group of geosynthetic encased stone columns," *J. Geotech. Geoenviron. Eng.*, vol. 136, no. 1, pp. 129–139, 2010. https://doi.org/10.1061/(asce)gt.1943-5606.0000187

[17] H. H. Baqir, M. F. Aswad, and M. Y. Fattah, "A numerical study on the behavior of stone columns with different area ratios in soft clays," *Int. J. GEOMATE*, vol. 26, no. 117, pp. 43–51, 2024. https://doi.org/10.21660/2024.117.4331

[18] Bentley Systems, *PLAXIS 3D Manual*, Delft, Netherlands, 2024. https://bentleysystems.service-now.com/community?id=kb_article_view&sysparm_article=KB0107989

[19] W. El Kamash and H. El Naggar, "Numerical simulation of the installation of vibro displacement columns in normally consolidated clay using a field case study," *Int. J. Geosynth. Ground Eng.*, vol. 7, no. 3, p. 54, 2021. https://doi.org/10.1007/s40891-021-00300-y

[20] T. Benz, R. Schwab, and P. Vermeer, "Small-strain stiffness in geotechnical analyses," *Bautechnik*, vol. 86, no. S1, pp. 16–27, 2009. https://doi.org/10.1002/bate.200910038

[21] M. K. Mohamed, M. A. Sakr, and W. R. Azzam, "Geotechnical behavior of encased stone columns in soft clay soil," *Innov. Infrastruct. Solut.*, vol. 8, no. 2, p. 80, 2023. https://doi.org/10.1007/s41062-023-01044-6

[22] M. X. Gu, H. Z. Mo, J. L. Qiu, J. Yuan, and Q. Xia, "Behavior of floating stone columns reinforced with geogrid encasement in model tests," *Front. Mater.*, vol. 9, p. 980851, 2022. https://doi.org/10.3389/fmats.2022.980851

[23] W. Yodsomjai, C. Phutthananon, P. Jongpradist, S. Keawsawasvong, and P. Jamsawang, "Optimal geogrid weight and failure modes of geogrid encased stone columns under axial compression loading with cost considerations," *Int. J. GEOMATE*, vol. 28, no. 128, pp. 125–132, 2025. https://doi.org/10.21660/2025.128.g14307

[24] M. Gaber, A. Kasa, N. Abdul-Rahman, and J. Alsharef, "Simulation of stone column ground improvement (comparison between axisymmetric and plane strain)," *Am. J. Eng. Appl. Sci.*, vol. 11, no. 1, pp. 129–137, 2018. https://doi.org/10.3844/ajeassp.2018.129.137

[25] T. Schanz, P. A. Vermeer, and P. G. Bonnier, "The hardening soil model: Formulation and verification," in *Beyond 2000 in Computational Geotechnics*. Routledge, 2019, pp. 281–296. https://doi.org/10.1201/9781315138206-27

[26] N. K. Al-Saoudi, M. M. Al-Qaissi, and S. E. Al-Baiaty, "Ordinary and encased stone columns with two different

relative densities," *Eng. Technol. J.*, vol. 31, no. 13, pp. 2415–2432, 2013. https://doi.org/10.30684/etj.31.13a.2

[27] R. R. Al-Omari, M. Y. Fattah, and H. A. Ali, "Behavior of swelling soil treated by grid geocell columns under a tank footing," *IOP Conf. Ser.: Mater. Sci. Eng.*, vol. 579, p. 012041, 2019. https://doi.org/10.1088/1757-899x/579/1/012041

[28] C. Yoo and D. Lee, "Performance of geogrid-encased stone columns in soft ground: Full-scale load tests," *Geosynth. Int.*, vol. 19, no. 6, pp. 480–490, 2012. https://doi.org/10.1680/gein.12.00033

[29] J. L. Briaud and P. Jeanjean, "Load settlement curve method for spread footings of sand," in *Vertical and Horizontal Deformations of Foundations and Embankments*. American Society of Civil Engineers, 1994, pp. 1774–1804.